24th COBEM - 2017

24th ABCM International Congress of Mechanical Engineering
December 3-8, 2017, Curitiba, PR, Brazil

# COBEM-2017-0124
# RESIDUAL THERMAL STRESS IN FUSED DEPOSITION MODELLING

**Rafael Quelho de Macedo**
**Rafael Thiago Luiz Ferreira**
Aeronautics Institute of Technology / GPMA - Research Group on Additive Manufacturing. DCTA ITA IEM, 12228-900, São José dos Campos, São Paulo, Brazil
rquelho@ita.br, rthiago@ita.br

***Abstract.*** *In this work, it is presented a model that simulates the process of FDM (Fused Deposition Modelling) capable of calculating temperature gradients and stresses (induced by the changes in temperature) during and after the filament deposition using FEM (finite element method). The stresses calculated vary in time during the printing process because the temperature is also changing, however stresses remain in the final printed part (residual thermal stress). It is shown that the intensity of those stresses are highly related to the rate of temperature changes during the printing process: the stresses are higher if the temperatures of the printed part vary rapidly. Those stresses can cause delamination during the deposition process and the residual thermal stresses can cause an offset to the failure envelope of the printed part. It is also shown that if the temperature of the 3D printer chamber is high, the printed part is subject to low temperature gradients during the printing process causing stresses of less intensity. This model is an useful tool for the industry, once it helps to explain how the printed part warps, to predict if it delaminates during the printing process and can estimate its strength.*

***Keywords:*** *3D printing, residual thermal stress, delamination, ABS*

## 1. INTRODUCTION

The fused deposition modelling (FDM) (Upcraft and Fletcher (2003a)) is a technique used in the raising field of 3D printing. In this additive manufacturing process, thin lines of a fused thermoplastic material are selectively deposited forming a desired component (Upcraft and Fletcher (2003b)) as exemplified in Fig.1. The FDM technology is already a reality in prototyping. However, new printing materials are evolving to render printed components of increased mechanical characteristics. Examples are thermoplastics reinforced by chopped carbon fibers (Ning *et al.* (2015)) and continuous carbon fibers embedded in nylon (Van Der Klift *et al.* (2016)). This broadens the FDM applicability to real components with structural functionality.

In order to create parts with mechanical responsibility using FDM, it is crucial to determine and evaluate the final mechanical properties of a printed part. In the recent literature, it has been reported that the mechanical properties of printed parts are highly related to the printing parameters (Mohamed *et al.* (2015); Lee *et al.* (2007)) such as raster angle, number of contours, air gap, layer thickness, etc. Moreover, due to the fusing process and the heat transfer during the printing process, residual thermal stresses arise. This influences the final geometry of the printed parts because of warping (Zhang and Chou (2008); Wang *et al.* (2007)), its failure envelope and also causing delamination during the printing process. The last phenomenon is related to the abrupt temperature changes that induce stresses high enough to trigger delamination between deposited layers. It can be seen in Fig.2 that a printed component delaminated (white part of Fig.2) when printed in an unclosed 3D printer (without chamber). Therefore, the part was exposed to the room temperature, and this caused faster changes in the deposited material temperature.

That being said, the objective of this work is to evaluate the residual thermal stresses due to the FDM process in two scenarios: a part printed in a closed 3D printer with heated bed and the same part printed in an unclosed 3D printer without heated bed.

## 2. METHODOLOGY

The finite element method (FEM) (Reddy (1996)) was employed to simulate the heat transfer during and after the printing process. The temperatures varying in time, calculated through a transfer heat analysis, were then used to calculate residual thermal stresses in the printed part, also using FEM.

In order to model the deposition process, small parts of the geometry were activated sequentially, according to the printing path, until the part was completely printed. A routine in Python was developed to generate the activation and deactivation of small portions of materials and to change boundary conditions in time according to the printing pattern.

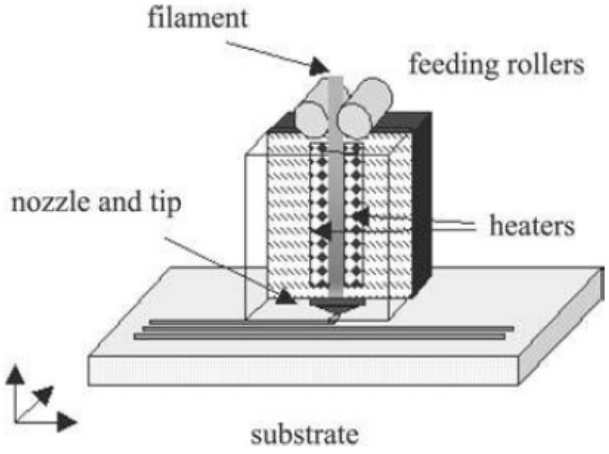


Figure 1. Illustration of the FDM process: Bellini and Güçeri (2003).

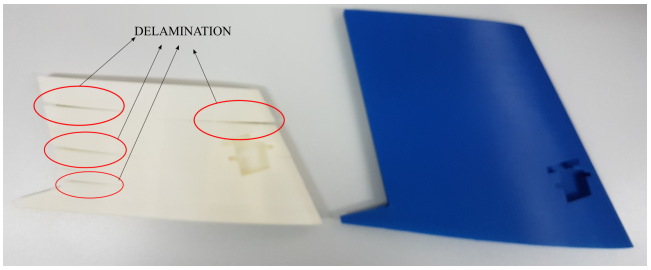


Figure 2. Delamination of ABS printed parts: left part printed in an unclosed 3D printer (without chamber) and right part printed in a closed 3D printer (with chamber).

The input of this routine is the geometry of the printed part, the printing pattern and printing speed.

Because of the activation procedure, the deposition process that is in reality a continuous phenomenon becomes discrete. The tinier the geometry is discretized, more the model represents a real deposition process. The commercial software ABAQUS was employed to model and simulate the transfer heat and the stress analysis. Below, it is presented in details the transfer heat and mechanical models.

### 2.1 Transfer heat analysis

The transient heat transfer problem is governed by Eq.(1) (Zhang and Chou (2006)):

$$\frac{\partial \rho c_p T}{\partial t} = \vec{\nabla} \cdot \left( \vec{k} \otimes \vec{\nabla} T \right) + q. \tag{1}$$

In Eq.(1), $\rho$, $c_p$ and $k$ are the density, specific heat and thermal conductivity of the printed filament, respectively. $T$ is the current solid temperature, $t$ is the current time, $\vec{\nabla}$ is the nabla operator, $q$ is the heat generated per unit volume. The operator $\otimes$ means element multiplication. It is worth mentioning that the printed material can have three different thermal conductivities, one for each direction: $\vec{k} = \{k_x \; k_y \; k_z\}^T$.

The newly activated geometry has an initial temperature equals to temperature of the extrusion nozzle, that it is the same as the melting temperature $T_m$ of the filament. Moreover, the portion of the printed part that is in contact with the print bed has its temperature $T_b$. During the printing process, the geometries that have already been printed lose heat to the 3D printer chamber (that has temperature $T_\infty$) by natural convection following the equation:

$$q = h(T - T_\infty). \tag{2}$$

In Eq.(2), $h$ is the convection coefficient for natural convection calculated considering the printed part as a plate according to Bergman *et al.* (2011). It is worth mentioning that $h$ is a function of the solid temperature $T$ that is in contact with the air chamber $T_\infty$.

During the printing process, because of the activation of geometries, the simulation time steps are divided according to: the geometry of the printed part, how many geometries the printed part has been divided (discretization) and also the printing velocity. For example, if a filament of length $L$ is being printed with velocity $V$ and it has been split in $n$ small geometries, then the simulation time steps are calculated by:

$$t_{\text{step}} = \frac{L}{nV}. \tag{3}$$

Moreover, during the printing process, each new activated geometry exchanges heat with the already activated geometries by conduction (Bergman *et al.* (2011)). It is also considered that the chamber temperature $T_\infty$ is constant during the printing process.

It can be seen in Fig.3 all concepts mentioned in the transfer heat simulation: at time $t$ of the simulation, the geometry has temperature $T_i$, loses heat to the chamber by convection and has temperature $T_b$ in the portion that is in contact to the printing bed; at the next simulation time step $(t + t_{\text{step}})$, the newly activated printed part has temperature $T_{i+1}$, both geometries lose heat to the chamber and also exchange heat between them due to conduction.

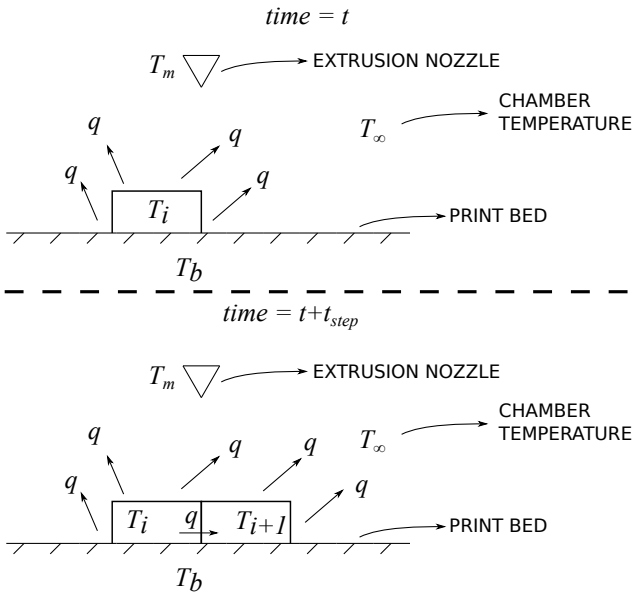


Figure 3. Two consecutives time steps of the heat transfer analysis during the printing process.

After the printing has finished, the chamber temperature ($T_\infty$) and the bed temperature ($T_b$) vary with time, decreasing their values to reach a specified value $T_{\text{final}}$.

### 2.2 Mechanical analysis

The temperature gradient calculated in the heat transfer analysis is now used to calculate stresses and strains. The changes in temperature induce a thermal strain according to Eq.(4):

$$\{\epsilon_{th}\} = \{\alpha(T)\}\,(T - T_{ref})\,. \tag{4}$$

In Eq.(4), $\{\epsilon_{th}\}$ are the thermal strains (using Voigt notation), $\{\alpha(T)\}$ is the coefficient of thermal expansion that is function of the temperature $T$ (current solid temperature) and $T_{ref}$ is a reference temperature. In this work, only isotropic filaments were studied, $\{\alpha(T)\}$ has only normal components, then the material only expands or contracts. Moreover, the filaments studied are polymers with a defined glass temperature $T_g$. Thus, it is considered in the analysis, that if $T_g \leq T \leq T_m$ then the filament is rather rubbery and it does not accumulate thermal strain, which only appears to temperatures $T < T_g$. Those ideas incorporated to Eq.(4) become:

$$\begin{aligned} \{\epsilon_{th}\} &= \{0\} \text{ if } T_g \leq T \leq T_m, \\ \{\epsilon_{th}\} &= \{\alpha(T)\}\,(T - T_g) \text{ if } T < T_g. \end{aligned} \tag{5}$$

The thermal strains of Eq.(5) are related to stresses and total strains by Eq.(6):

$$\{\sigma\} = [D]\,(\{\epsilon\} - \{\epsilon_{th}\})\,. \tag{6}$$

In Eq.(6), $\{\sigma\}$ is the stress vector, $[D]$ is the constitutive matrix and $\{\epsilon\}$ is the total strain vector. Once more, FEM was employed to calculate the total strains and stresses for each time step due to the temperature changes.

During the printing process, the nodes that are in contact with the table have their displacement constrained. After the printing has finished, in order to simulate the removal of the printed part from the print bed, those boundary conditions are gradually released to let the printed part to warp and the thermal residual stresses on final printed part to be calculated.

It is worth mentioning that when the print bed is removed, there are no more boundary conditions in the mechanical analysis. However, residual thermal stresses remain in the printed part. This happens because each new portion of newly deposited material becomes a restriction to expansion or contraction to the already deposited material.

## 3. RESULTS

Two different scenarios were analysed in order to explain possible causes of the delamination depicted in Fig.2. In the first analysis, the simulation considered the presence of a 3D printer chamber that induces a higher $T_\infty$ and also bed temperature equal to the printed material $T_g$. In the second analysis, the same part was printed without a 3D printer chamber (lower $T_\infty$) and also bed temperature equal to $T_\infty$ (no heated bed).

The mechanical and thermal properties of the ABS used in those analyses are depicted in Tab.1. The Young's modulus presented in Tab.1 is referred to the ABS in a wire form, not printed yet.

Table 1. Mechanical and thermal properties of ABS.

| Property | Value |
|---|---|
| $k\ (W/mK)$ - Zhang and Chou (2006) | 0.19 |
| Specific heat $(kJ/kgK)$ - Zhang and Chou (2006) | |
| At $0°C$ | 1.62 |
| At $105°C$ | 1.62 |
| At $130°C$ | 3 |
| At $280°C$ | 1.68 |
| $\rho\ (kg/m^3)$ - Zhang and Chou (2006) | 1200 |
| $\alpha\ (\mu m/mK)$ - Zhang and Chou (2006) | 80 |
| $\nu$ - Zhang and Chou (2006) | 0.4 |
| Young's modulus $(GPa)$ - Casavola *et al.* (2016) | 1.81 |

The part printed has dimensions and printing path as depicted in Fig.4. The printed part was divided in small geometries of dimensions $4$ x $0.3$ x $0.33$ mm that were activated during the simulation according to the printing path. The layer height is $0.3$ mm (total of 4 deposited layers) and the road width is $0.33$ mm. The printing velocity in the $x$ direction was set to be $V_x = 32mm/s$. It can be concluded from Eq.(3) that the time step for the analysis is: $t_{\text{step}} = \frac{40}{\frac{40}{4}32} = 0.125s$. Each geometry was discretized with 8 finite elements: 2 elements in $x$, 2 elements in $y$ and 2 elements in $z$. In the transfer heat analysis, the 8-node linear heat transfer brick DC3D8 element was used, and for the mechanical analysis the 20-node quadratic brick C3D20 element was used. In order to be concise, the stress results shown below are depicted in respect of the von Mises invariant of the stress tensor.

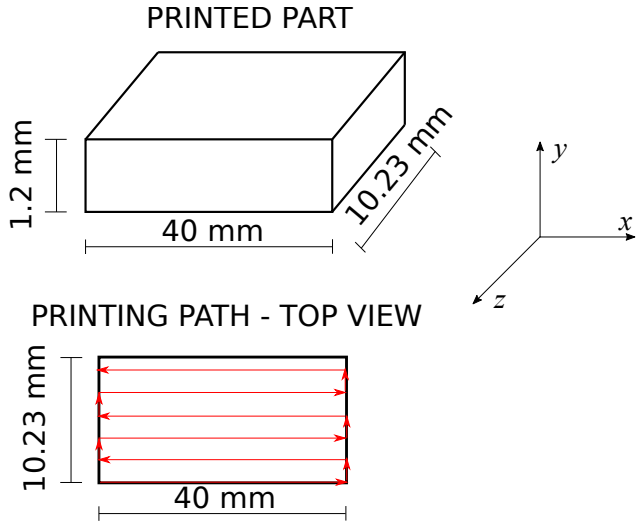


Figure 4. Printed part dimensions and the printing path deposition.

### 3.1 First scenario

It was considered the presence of a 3D printer chamber and also a heated print bed in this analysis. During the printing process, the chamber temperature was $T_\infty = 75°C$ and bed temperature of $T_b = T_g = 110°C$. After the deposition process had finished, the chamber temperature dropped to $T_\infty = 25°C$ in $3.5min$ and the the bed temperature dropped to $T_b = 25°C$ in around $7min$. The initial temperature for the newly activated geometry was $T_m = 235°C$ (melting temperature for ABS).

Figure 5 (a) shows the von Mises stresses calculated at the end of the deposition process, when the print bed was still holding the printed part. Later, after the printed part reached equilibrium to the environment temperature, the bed boundary conditions were removed and the residual thermal stresses were calculated, which are shown in Fig.5 (b). It can be seen that when the print bed is removed, the stresses are lowered, but there is still residual thermal stress in the final printed part.

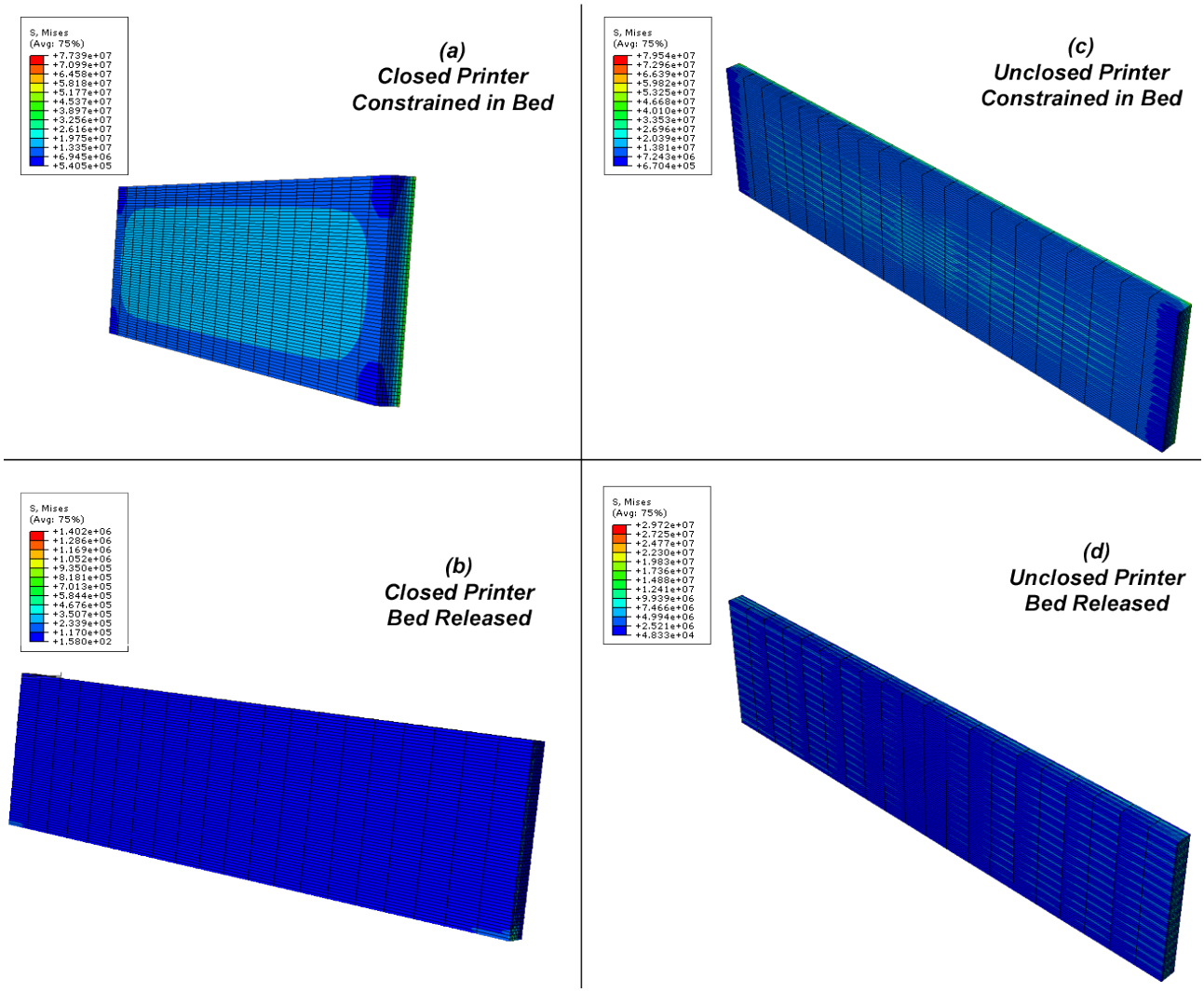


Figure 5. First and second scenarios von Mises stress distribution.

### 3.2 Second scenario

In this scenario, it was considered that there was not a 3D printer chamber, causing abruptly temperature changes. During the printing process, the chamber temperature was $T_\infty = 35°C$ and bed temperature of $T_b = 35°C$. Those temperatures were chosen because the environment temperature was $35°C$, and it was considered that the extrusion process heated the environment near to the printed part. After the deposition process had finished, the chamber temperature dropped to $T_\infty = 25°C$ in $3.5min$ and the bed temperature dropped to $T_b = 25°C$ in $3.5min$ as well. The initial temperature for the newly activated geometry was $T_m = 235°C$ (melting temperature for ABS).

Figure 5 (c) shows the von Mises stresses calculated at the end of the deposition process, when the print bed was still holding the printed part. Later, after the printed part reached equilibrium to the temperature environment, the bed

boundary conditions were removed and the residual thermal stresses were calculated, which can be seen in Fig.5 (d). Similar to what happened in the last analysis, after the print bed has been removed, the stresses were lowered, but residual thermal stress still remains in the final printed part.

## 4. CONCLUSIONS

It can be seen from the results above that the second scenario (without 3D printer chamber and no heated bed) yielded higher stresses than the first scenario (with 3D printer chamber and heated bed). In the first scenario, the heated print bed with temperature $T_b = T_g$ and the 3D printer chamber did not allow abrupt temperature changes during the deposition process, yielding stresses with less intensity.

On the other hand, the printing process in an unclosed 3D printer (without chamber) and without heated print bed caused higher stresses, as depicted in the second scenario results. In this kind of printing process, the printed part is subjected to rapidly temperature changes yielding higher stresses during and after (residual thermal stress) the printing process.

The results presented in this paper can explain why some printed parts delaminate or warp. Those two phenomena are related to the intensity of the stress fields, which are caused by temperature changes in the printing process. Then, in order to prevent delamination or lessen the warping, a careful analysis on the temperature changes during the printing process should be made. The model presented in this paper can be used for that purpose. Moreover, the residual thermal stresses can be used to analyse the failure behaviour of printed parts and also to determine how the printing parameters affect their strength.

## 5. ACKNOWLEDGEMENTS

This work was supported by grants from FAPESP Process 2016/17835-6 and 2015/00159-5.

## 6. REFERENCES

Bellini, A. and Güçeri, S., 2003. "Mechanical characterization of parts fabricated using fused deposition modeling". *Rapid Prototyping Journal*, Vol. 9, No. 4, pp. 252–264.

Bergman, T.L., Incropera, F.P., DeWitt, D.P. and Lavine, A.S., 2011. *Fundamentals of heat and mass transfer*. John Wiley & Sons.

Casavola, C., Cazzato, A., Moramarco, V. and Pappalettere, C., 2016. "Orthotropic mechanical properties of fused deposition modelling parts described by classical laminate theory". *Materials & Design*, Vol. 90, pp. 453–458.

Lee, C., Kim, S., Kim, H. and Ahn, S., 2007. "Measurement of anisotropic compressive strength of rapid prototyping parts". *Journal of materials processing technology*, Vol. 187, pp. 627–630.

Mohamed, O.A., Masood, S.H. and Bhowmik, J.L., 2015. "Optimization of fused deposition modeling process parameters: a review of current research and future prospects". *Advances in Manufacturing*, Vol. 3, No. 1, pp. 42–53.

Ning, F., Cong, W., Qiu, J., Wei, J. and Wang, S., 2015. "Additive manufacturing of carbon fiber reinforced thermoplastic composites using fused deposition modeling". *Composites Part B: Engineering*, Vol. 80, pp. 369–378.

Reddy, J.N., 1996. *An introduction to the finite element method*. McGraw-Hill, New York, 2nd edition.

Upcraft, S. and Fletcher, R., 2003a. "The rapid prototyping technologies". *Assembly Automation*, Vol. 23, No. 4, pp. 318–330.

Upcraft, S. and Fletcher, R., 2003b. "The rapid prototyping technologies". *Assembly Automation*, Vol. 23, No. 4, pp. 318–330.

Van Der Klift, F., Koga, Y., Todoroki, A., Ueda, M., Hirano, Y., Matsuzaki, R. *et al.*, 2016. "3d printing of continuous carbon fibre reinforced thermo-plastic (cfrtp) tensile test specimens". *Open Journal of Composite Materials*, Vol. 6, No. 01, p. 18. doi:http://dx.doi.org/10.4236/ojcm.2016.61003.

Wang, T.M., Xi, J.T. and Jin, Y., 2007. "A model research for prototype warp deformation in the fdm process". *The International Journal of Advanced Manufacturing Technology*, Vol. 33, No. 11-12, pp. 1087–1096.

Zhang, Y. and Chou, K., 2008. "A parametric study of part distortions in fused deposition modelling using three-dimensional finite element analysis". *Proceedings of the Institution of Mechanical Engineers, Part B: Journal of Engineering Manufacture*, Vol. 222, No. 8, pp. 959–968.

Zhang, Y. and Chou, Y., 2006. "Three-dimensional finite element analysis simulations of the fused deposition modelling process". *Proceedings of the Institution of Mechanical Engineers, Part B: Journal of Engineering Manufacture*, Vol. 220, No. 10, pp. 1663–1671.

## 7. RESPONSIBILITY NOTICE

The authors are the only responsible for the printed material included in this paper.